Advanced Composites and Hybrid Materials (2022) 5:2339–2352
https://doi.org/10.1007/s42114-022-00424-3

ORIGINAL RESEARCH

Direct growth of cobalt-doped molybdenum disulfide on graphene nanohybrids through microwave irradiation with enhanced electrocatalytic properties for hydrogen evolution reaction

Shatila Sarwar[1] · Mao-Chia Lin[1] · Md Robayet Ahasan[2] · Yifan Wang[2] · Ruigang Wang[2] · Xinyu Zhang[1]

Received: 30 July 2021 / Revised: 13 January 2022 / Accepted: 17 January 2022 / Published online: 8 February 2022

Abstract

Molybdenum disulfide (MoS_2) nanosheets are promising candidates as electrode materials for the efficient hydrogen production through water splitting. However, their activities are only governed by the edge sites, and their charge transfer efficiencies are still unsatisfactory. Defect generation and hybridization are two very effective ways to tune the nanostructures of MoS_2 and enhance their electrocatalytic properties. Herein, cobalt-doped molybdenum disulfide (Co-MoS_2) nanosheets have been synthesized on graphene network (Co-MoS_2/G) by an ultrafast, facile, and reliable microwave irradiation technique. The structural, morphological, and compositional properties were characterized for these Co-MoS_2/G composites. The compositionally optimized catalyst of as-produced Co-MoS_2/G delivers excellent hydrogen evolution reaction (HER) performance in acidic medium with the best combination of three major parameters, resulting in a low overpotential of 78.1 mV, a small Tafel slope of 40.0 mV per decade, and a high exchange current density of 0.0917 mA cm^{-2}, which also exhibits excellent electrochemical stability for 5000 cycles with negligible loss of the cathodic current and long-term durability for 94 h. Co-doping greatly enhanced the intrinsic activity of MoS_2 nanosheet catalyst by creating abundant defects, and in addition, the integration of graphene notably promoted the electrical conductivity and mechanical properties of Co-MoS_2/G composites. This study would supply an ultrafast, simple, and efficient strategy for developing excellent metal-doped electrocatalysts for HER.

Keywords Co-doped MoS_2 · Graphene · Microwave irradiation · Hydrogen evolution reaction

1 Introduction

In present days, hydrogen (H_2) is extensively being generated by steam and oil reforming processes. However, there is a growing interest in increasing the share of hydrogen production through water electrolysis in order to avoid the use of carbon-based sources [1–3]. Electrochemical water splitting offers an environmentally suitable and technologically promising approach to produce useful hydrogen fuel that can comply with future energy demand [4, 5]. To achieve the optimal performance in water splitting, efficient cathode catalysts are required for hydrogen evolution reaction (HER). As known, platinum (Pt) and Pt-group metals are the most electroactive catalysts, but the rareness and high costs limit their large-scale commercial utilization. Therefore, many researchers are currently focusing on developing highly effective HER catalysts based on the earth-abundant elements [5–7]. A combination of high surface area, high conductivity, fast charge transfer ability, excellent intrinsic activity, promising stability, material abundancy, and low material cost is universally desired for potential HER catalysts. Noble metal-free compounds, such as transition-metal oxides, chalcogenides, carbides, nitrides, phosphides, etc. have been studied vigorously as electrocatalysts for hydrogen generation [8–13]. Recently, the transition-metal dichalcogenides (MX_2, M = Mo, W, Zn, Fe, etc. and X = S, Se, Te) have drawn much attention as efficient HER catalysts [14–16]. Among them, molybdenum disulfide (MoS_2) has received exceptional attention due to the low hydrogen adsorption free energy ($\Delta G_H^* \approx 0$) on catalyst surface,

✉ Ruigang Wang
rwang@eng.ua.edu

✉ Xinyu Zhang
xzz0004@auburn.edu

[1] Department of Chemical Engineering, Auburn University, Auburn, AL 36849, USA

[2] Department of Metallurgical and Materials Engineering, The University of Alabama, Tuscaloosa, AL 35487, USA

which makes it a promising alternative to the Pt catalysts [8, 17, 18]. Nevertheless, low conductivity, inadequate active sites, restacking of MoS_2 sheets, and the inert S atoms in plane sites make it difficult to achieve high efficiency for hydrogen generation. To overcome these shortcomings, extensive studies have been set forth to develop several nanostructures of MoS_2-based compounds, such as nanoparticles, nanosheets, nanoribbons, core-shells, etc. [19–24]. In addition to the structural optimizations, defect incorporations have also been widely established and acclaimed to enhance the intrinsic activity of MoS_2, such as hybridization with carbon-based materials [25–27], hybridization with other materials (cadmium sulfide and vanadium sulfide) [28–30], substitutional doping [31–33] and 2H to 1T phase conversion [34, 35], etc. Among them, doping with metal elements (such as Co, Fe, Au, Ni, Pt, etc.) is a facile method to achieve structural and/or chemical modifications [31, 36–40]. For instance, Dai et al. investigated Co-doping into the MoS_2 nanosheets, which claimed the formation of Co-doped MoS_2 with higher surface area, higher number of active sites, and substantially superior HER activity than pure MoS_2 counterparts, resulting in the overpotential (η) of 135 mV, Tafel slope of 50 mV dec^{-1}, and i_0 of 0.03 mA cm^{-2} [41]. Bose et al. demonstrated that the doping of Co atom in pristine MoS_2 can serve as additional active sites, further enhancing the HER performance with η of 218 mV, Tafel slope of 50 mV dec^{-1}, and i_0 of 0.0005 mA cm^{-2} [42]. Very recently, Ma et al. reported a hydrothermal method to generate bifunctional catalyst of Co-doped MoS_2 uniformly dispersed on reduced graphene oxide (rGO) both for HER and oxygen evolution reaction (OER) [43]. The HER performance reveals the η of 147 mV and Tafel slope of 49.5 mV dec^{-1}. This enhanced HER performance was attributed to the synergetic effects of Co, MoS_2, and rGO by high conductivity and interconnectivity, which formed abundant defects and accelerated the electron transfer. Several doping methods have been developed in recent years [44–49]. Moreover, to overcome the poor charge transfer ability of transition-metal–doped MoS_2, carbonaceous materials (such as graphene, carbon nanotubes, rGO, etc.) have been widely applied in the fabrication of HER catalysts due to their large specific surface area, superior electronic conductivity, and good stability [33, 50–52]. Besides, carbonaceous materials have been widely used in the latest research fields [53–60]. Despite the progress in recent works, large-scale fabrication of Co-doped MoS_2 catalysts with improved activity and durability properties still faces several practical challenges due to the complex and time-consuming synthesis methods, such as hydrothermal, solvothermal, CVD, etc. To overcome these complexities, based on our previous works [11, 61, 62], we propose to fabricate cobalt-doped molybdenum sulfide nanosheets on graphene network (Co-MoS_2/G) by an ultrafast (60 s), facile, reliable, and scalable microwave irradiation process. To the best of our knowledge, this is the first time our work demonstrates such a simple microwave-assisted synthesis of non-noble metal-doped MoS_2/G to be employed as HER electrocatalyst. It is expected that the synergistic effect of Co, MoS_2, and graphene endows the composites with excellent HER activity, good charge transfer ability, along with long-term stability. Besides, acting as an intertwined network for anchoring the Co-MoS_2 nanosheets, graphene plays a crucial role during microwave-initiated heating, acting as a microwave susceptor. To determine the HER activities of electrocatalysts, considering the three major parameters, it is important to have low overpotential, small Tafel slope, and high exchange current density. However, most of the previous works struggle to achieve a good combination of these three parameters [41–43]. In this regard, our results reveal that the compositionally optimized Co-MoS_2/G exhibits enhanced electrocatalytic activity comparing to the undoped MoS_2/G with η of 78.1 mV, Tafel slope of 40.0 mV dec^{-1}, i_0 of 0.0917 mA cm^{-2}, and excellent durability, which are superior to the most previously reported Co-doped MoS_2-based electrocatalysts. To the best of our knowledge, this is the best combination of three of the major parameters so far for the Co-doped MoS_2-based electrocatalysts.

2 Methodology

2.1 Materials and reagents

Cobalt carbonate ($CoCO_3$) and ammonium tetrathiomolybdate ($(NH_4)_2MoS_4$) precursors were obtained from Alfa Aesar and BeanTown Chemical, Inc., respectively. Graphene was acquired from Magnolia Ridge Inc. A total of 10 wt.% Pt/C catalyst was purchased from Sigma-Aldrich, Inc. For electrochemical characterizations, Ag/AgCl (3 M KCl) reference electrode was purchased from Hach, graphite rod (5 mm diameter) was obtained from Alfa Aesar, and glassy carbon electrode (3 mm diameter) was purchased from CH Instruments, Inc. All chemicals were of analytical grades and applied without further purification.

2.2 Preparation of catalyst samples

To prepare the Co-MoS_2/G compounds, commercial powders of $CoCO_3$, $(NH_4)_2MoS_4$, and graphene were mixed with CS_2 solvent homogeneously in a 20-mL scintillation vial based on the different ratio shown in Table 1. After that, the vial was air dried and positioned inside a microwave oven, then electromagnetically irradiated for 60 s at the power of 1250 W. During the process, graphene absorbs the microwave energy and generates thermal energy (~ 1000 ℃) by resistive heating, which can trigger the vigorous reactions among precursors. Five different Co-MoS_2/G composites were

Table 1 Different amounts of precursors to synthesize the microwave-irradiated hybrid catalysts

Samples	$CoCO_3$ (mg)	$(NH_4)_2MoS_4$ (mg)	CS_2 (μL)	Graphene (mg)	Microwave power (W)	Microwave time (s)
Co-MoS_2/G-1	1	15	50	15		
Co-MoS_2/G-3	3	15	50	15		
Co-MoS_2/G-5	5	15	50	15		
Co-MoS_2/G-8	8	15	50	15	1250	60
Co-MoS_2/G-10	10	15	50	15		
CoS_2/G	5	–	50	15		
MoS_2/G	–	15	50	15		
CoO_x/G	5	–	–	15		

prepared by tailoring the amount of Co-loading from 1 to 10 mg. Following the similar steps, CoS_2/G composite was prepared except adding $(NH_4)_2MoS_4$ precursor, and MoS_2/G composite was synthesized except adding the $CoCO_3$ precursor (Table 1). In addition, to compare the HER performances, CoO_x/G composite was also synthesized through microwave irradiation.

2.3 Materials characterizations

The morphologies and chemical compositions of catalyst samples were determined by scanning electron microscope (SEM; Apreo FE) connected with an energy-dispersive X-ray spectrometer (EDS, EDAX Instruments) applying the 20 kV acceleration voltage. Additionally, transmission electron microscope (TEM, FEI Tecnai F20) was used for further analysis at 200 kV. The crystal structures were investigated by the powder X-ray diffraction (XRD) on a Philips X'pert MPD diffractometer with Cu Kα radiation ($\lambda = 1.54056$ Å) at 45 kV and 40 mA. Furthermore, to determine the chemical states and compositions of catalyst samples, X-ray photoelectron spectroscopy (XPS) analysis was performed on a Kratos Axis Ultra DLD spectrometer applying a monochromatic Al Kα radiation under UHV condition.

2.4 Electrochemical characterizations

To prepare a catalyst ink, 50 mg of active material was uniformly mixed with 5 mg of PVDF (polyvinylidene fluoride) and 2.5 mL of DMF (*N*, *N*-dimethylformamide) by 20 min of sonication. Then, 20 μL of each catalyst ink was loaded onto the clean surface of glassy carbon electrode (GCE, 3 mm in diameter) maintaining a consistent mass loading of around 1 mg cm^{-2} for each sample and vacuum dried at 60 °C for 30 min. A three-electrode setup was used to perform the tests consisting of a catalyst-modified GCE as working electrode, Ag/AgCl (3 M KCl) as reference electrode, and a graphite rod as counter electrode in 0.5 M H_2SO_4 acidic electrolyte. Measured potentials were referred to the reversible hydrogen electrode (RHE) based on the equation, $V\,(vs.\ \mathrm{RHE}) = V_{\mathrm{measured}}\,(vs.\ \mathrm{Ag/AgCl}) + 0.197 + (0.059 \times \mathrm{pH})$. Therefore, prior to each of the test, the pH value was measured using a benchtop pH meter.

3 Results and discussion

3.1 Structural and compositional investigations

The SEM and TEM micrographs (Fig. 1a and b) show that the as-prepared Co-doped MoS_2 nanosheets are almost uniformly distributed on graphene flakes. The HRTEM images of Fig. 1c and d suggest that the catalyst is composed of multiple layers with an interlayer distance of 0.63 nm, corresponding to the (002) plane of MoS_2 nanosheet. It also shows significant defects in MoS_2 layers due to the Co-doping in Fig. 1d, which are not present in the undoped-MoS_2/G (Fig. 1c). In Fig. 1e–i, the elemental distribution of Co-MoS_2/G-5 for the C, Mo, S, and Co species is displayed, respectively. Figure 1i shows that the Co element is distributed uniformly in Co-doped MoS_2 composite, which as well confirms that the Co element is successfully doped into MoS_2.

Besides elemental distributions, EDS analysis was also performed for the qualitative analysis and to determine the contents of Co-MoS_2/G nanocomposites. Figure 2a and Fig. S1 show the EDS results scanning on the surface of as-produced Co-MoS_2/G samples with different Co precursor amounts. They illustrate that the atomic ratios of Co: Mo: S in the samples of Co-MoS_2/G-1, Co-MoS_2/G-3, Co-MoS_2/G-5, Co-MoS_2/G-8, and Co-MoS_2/G-10 are about 0.25: 1.0: 2.25, 0.45: 1.0: 1.99, 0.31: 1.0: 1.74, 1.19: 1.0: 2.10, and 0.71: 1.0: 1.79, respectively, which further confirms the direct growth of Co-contained MoS_2 on graphene. However, the relative contents of Co and Mo are inconsistent with an increase in the amount of Co doping, which could be due to the semi-quantitative analysis performed by EDS tests that may not provide the exact elemental analysis. In

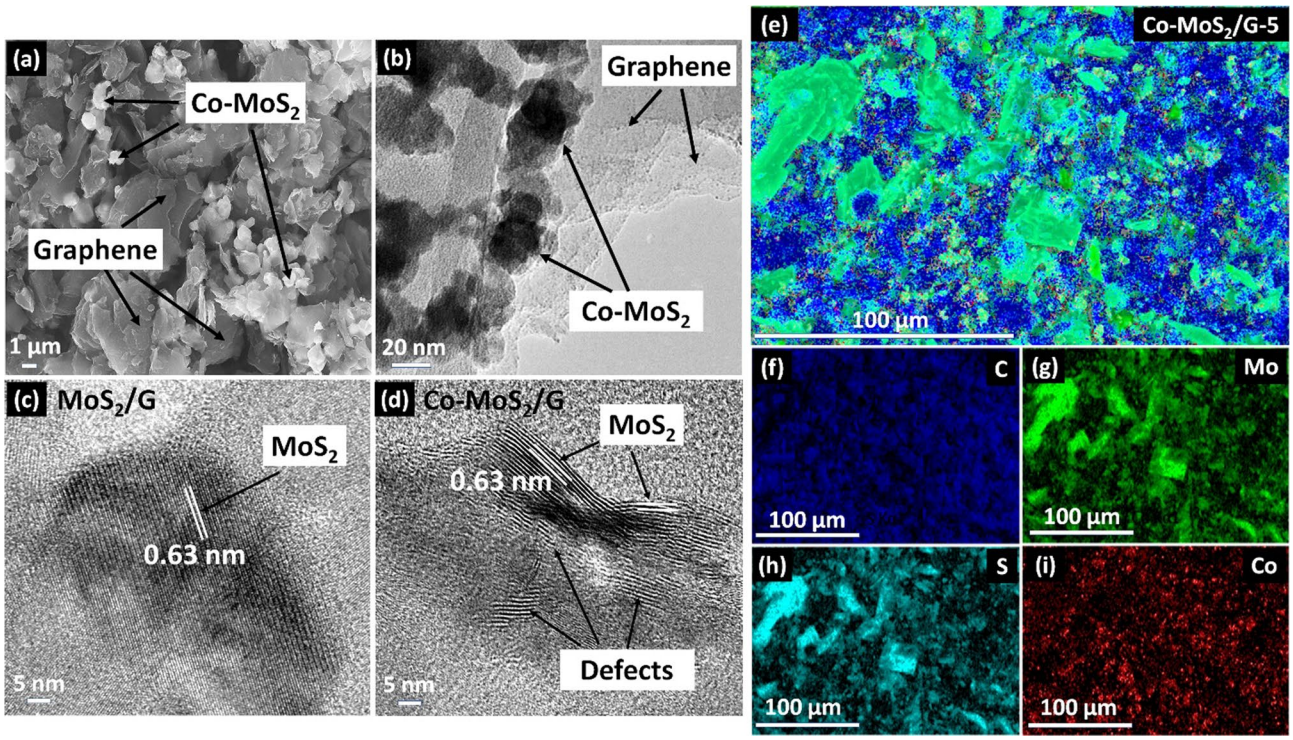

Fig. 1 **a** SEM, **b** TEM images of Co-MoS_2/G-5. HRTEM micrographs of **c** MoS_2/G composite, **d** Co-MoS_2/G-5 composite. **e** EDS elemental mapping of Co-MoS_2/G-5 composite. **f–i** Elemental distributions of carbon (C), molybdenum (Mo), sulfur (S), and cobalt (Co) species, respectively

addition, Fig. 2b shows the XRD patterns of five different Co-MoS_2/G samples, MoS_2/G, and CoS_2/G samples. All the curves display a high intensity peak at ~ 26° as a reflection from carbon layers (002) of graphene. The peaks appearing in Co-MoS_2/G samples and MoS_2/G at 14.2°, 35.2°, 46.8°, 54.4°, and 58.5° are corresponding to (002), (100), (104), (106), and (110) planes, respectively, indexed to hexagonal crystalline MoS_2 (JCPDS card No. 37–1492) [63]. Based on the Bragg's law, the (002) plane at $2\theta = 14.2°$ results an interlayer spacing of 0.628 nm, which also matches with the TEM demonstration in Fig. 1. The existence of polycrystalline $2H - MoS_2$ phase is demonstrated in Fig. S2. The results confirm the synthesis of high-purity Co-MoS_2/G and MoS_2/G composites since no impurity peaks were detected,

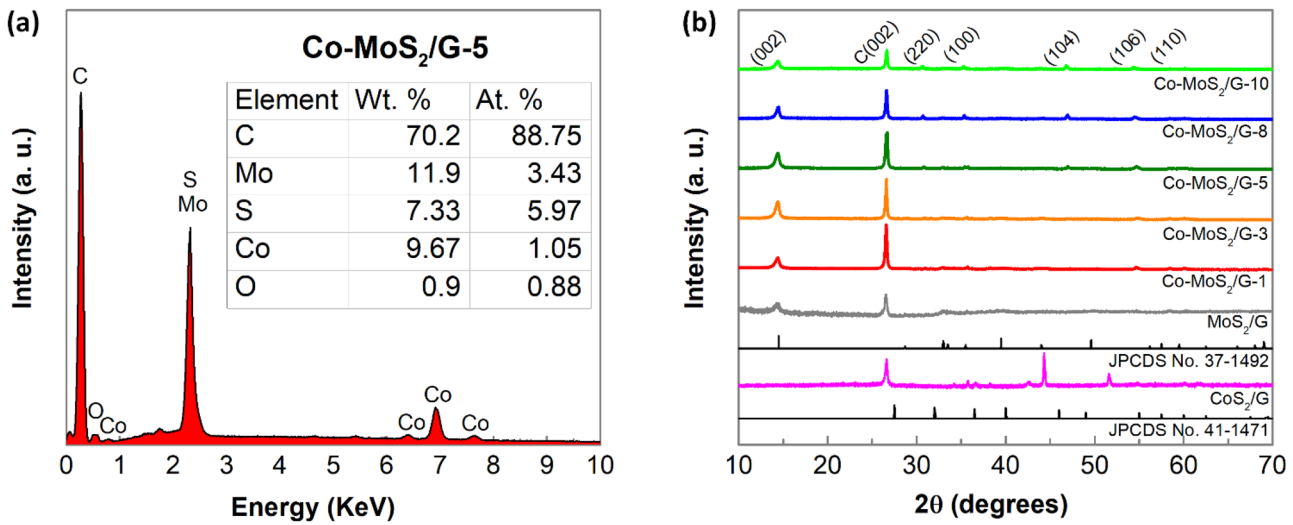

Fig. 2 **a** EDS compositional analysis of Co-MoS_2/G-5. **b** XRD patterns for Co-MoS_2/G, MoS_2/G, and CoS_2/G nanocomposites

except only a peak at 30.6° corresponding to CoO_x [64]. The XRD patterns were also compared with CoS_2/G composite. The results indicate that Co element is effectively doped into MoS_2 instead of forming CoS_2 phase, since the XRD pattern of CoS_2 does not match with the resultant Co-MoS_2/G nanocomposites. Similar to Co-MoS_2/G nanocomposite, CoS_2/G shows an impurity peak of CoO_x at around 44.5° [65].

X-ray photoelectron spectroscopy (XPS) was further employed to characterize the chemical states of as-synthesized Co-MoS_2/G-5 nanocomposite. As shown in survey spectrum in Fig. 3a, two additional peaks were found at around 781.1 eV and 798.9 eV, which are assigned to Co species [66]. It also reveals the atomic ratio of Co: Mo: S is around 0.4: 1.0: 2.4, which closely matches with the EDS result. Figure 3b–d demonstrate the Co 2p, Mo 3d, and S 2p XPS spectra of Co-MoS_2/G-5, respectively. As shown in Fig. 3b, the high-intensity peaks appeared at 778.4 eV and 793.5 eV correspond to Co $2p_{3/2}$ and Co $2p_{1/2}$, respectively, which are assigned to Co^{2+}. This indicates that Co ions are present in the MoS_2 lattice as a form of CoMoS phase [41, 63]. To further confirm the presence of Co-doping, the binding energy difference analysis was performed, which involves evaluating the binding energy differences ($\Delta E_1 - \Delta E_2$). Here, $\Delta E_1 = E_{Co\ 2p3/2} - E_{S\ 2p3/2}$, and $\Delta E_2 = E_{Mo\ 3d5/2} - E_{S\ 2p3/2}$. In this study, $\Delta E_1 = (778.4 - 161.8)$ eV = 616.6 eV and $\Delta E_2 = (228.9 - 161.8)$ eV = 67.1 eV, which matches with previously reported value of 67.2 eV, specifying that CoMoS is the major participating phase [67]. In addition, the peaks at 781.4 eV and 797.5 eV belong to the oxidized Co^{2+}. The rest of the peaks at 784.7 eV and 802.7 eV are derived from the extended peak satellite signal [63]. In Fig. 3c, the peaks at 228.9 eV and 232.1 eV are corresponded to Mo $3d_{5/2}$ and Mo $3d_{3/2}$, respectively, suggesting the oxidation state of Mo^{4+} [68]. In addition, a weak peak at 226.3 eV is attributed to S 2s orbital,

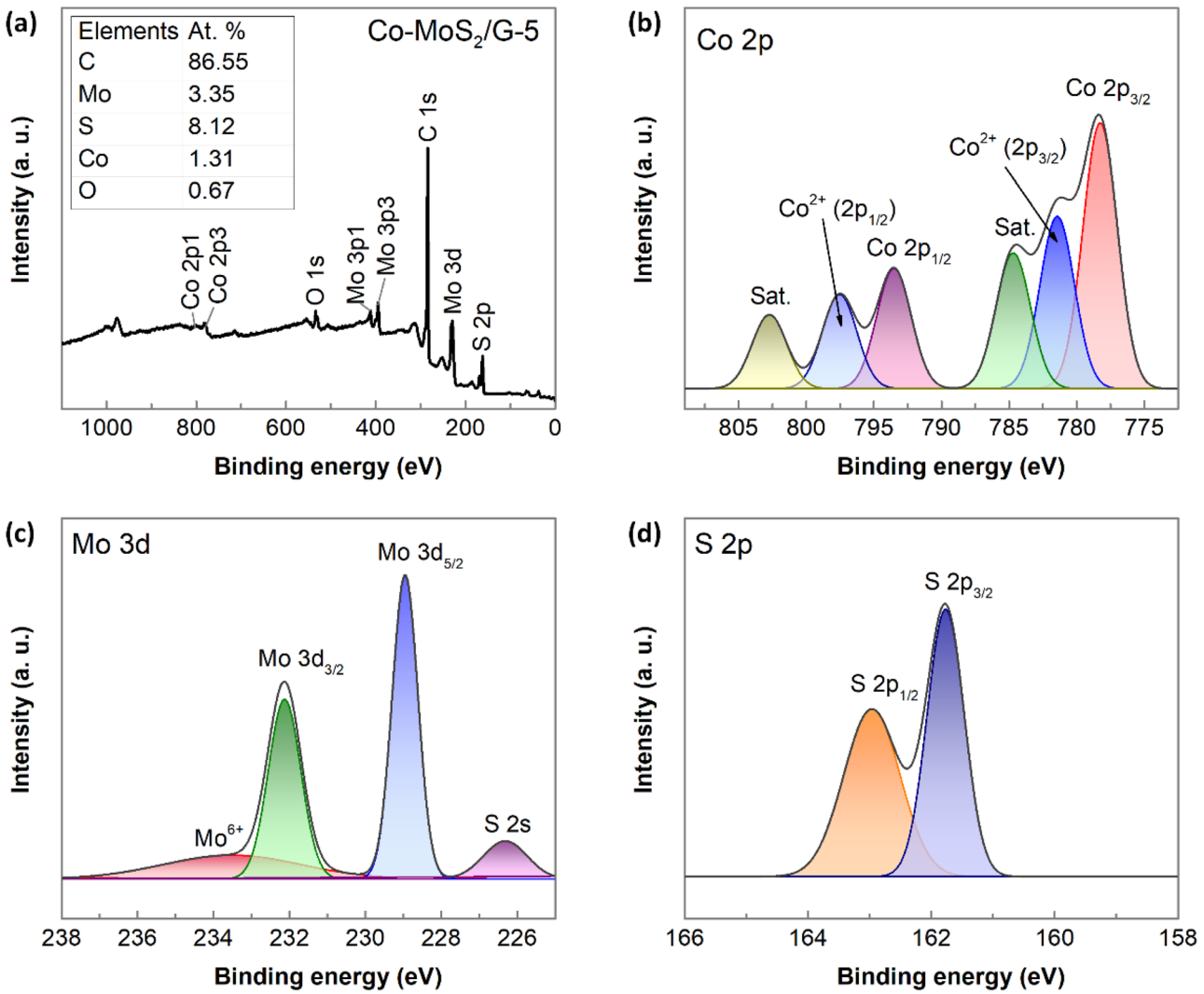

Fig. 3 **a** XPS survey spectrum of Co-MoS_2/G-5 composite. **b–d** High-resolution XPS spectra for Co 2p, Mo 3d, and S 2p regions, respectively

which confirms the formation of MoS_2 [68]. As shown in Fig. 3d, the S 2p spectrum exhibits two peaks at 161.8 eV and 162.9 eV, which are assigned to the spin–orbit coupling of S $2p_{3/2}$ and S $2p_{1/2}$, respectively [66]. Likewise, the XPS analysis was performed for MoS_2/G sample, which is displayed in Fig. S3. Based on these results, it clearly shows that the Co is effectively doped into MoS_2 lattice in the microwave-irradiated samples of Co-MoS_2/G.

3.2 Electrocatalytic activities of catalyst samples

To investigate the HER activities of the as-prepared samples, LSVs were carried out at 2 mV s^{-1} in 0.5 M H_2SO_4 electrolyte at room temperature. Figure 4a displays the polarization curves of Co-MoS_2/G samples with different Co-loading (1, 3, 5, 8, and 10 mg), where Co-MoS_2/G-5 with 5 mg of Co-loading exhibits the lowest overpotential (η) of 78.1 mV to reach the current density of 10 mA cm^{-2}. The HER activity improves gradually with the increase in cobalt (Co) from 1, 3, and 5 mg for Co-MoS_2/G-1 (Co: Mo = 0.51: 2.04), Co-MoS_2/G-3 (Co: Mo = 0.96: 2.12), and Co-MoS_2/G-5 (Co: Mo = 1.05: 3.43) samples, respectively. However, the activity decreases for further increase in Co-loading (8 and 10 mg) for Co-MoS_2/G-8 (Co: Mo = 2.01: 1.68) and Co-MoS_2/G-10 (Co: Mo = 3.17: 4.49) samples. This may happen due to the excess amount of cobalt oxide, CoO_x (electrocatalytically less active, shown in Fig. 4b) decomposed from $CoCO_3$ precursor, or the precursor remains unreacted in the nanocomposites. Due to the best results found from Co-MoS_2/G-5 sample, it was selected to carry out the other electrochemical characterizations and comparisons. As shown in Fig. 4b, it can be clearly observed that the bare GCE, graphene, and CoS_2/G samples do not possess any significant HER activity,

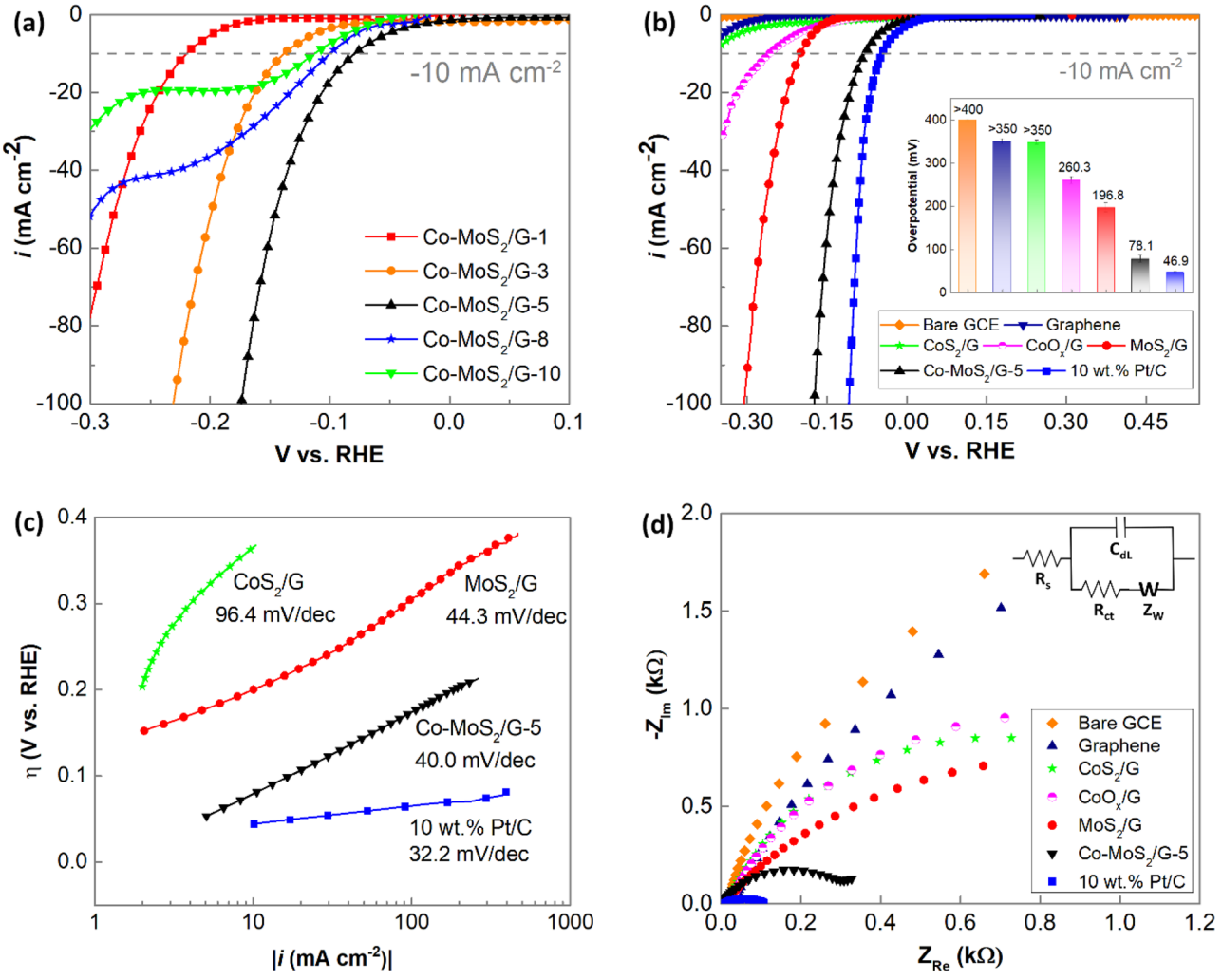

Fig. 4 **a** LSVs for Co-MoS_2/G samples. **b** LSVs for bare GCE, graphene, CoS_2/G, CoO_x/G, MoS_2/G, Co-MoS_2/G-5, and 10 wt.% Pt/C catalysts. [Inset: overpotentials of the subsequent catalyst samples]. **c** Tafel slopes for CoS_2/G, MoS_2/G, Co-MoS_2/G-5, and 10 wt.% Pt/C. **d** Nyquist plots at the overpotential of 150 mV *vs.* RHE

Table 2 Major electrochemical parameters of Co-MoS_2/G-5 nanocomposite, comparing with graphene, as-produced CoS_2/G, CoO_x/G, MoS_2/G samples, and 10 wt.% Pt/C catalyst

Samples	η at 10 mA cm^{-2} (mV *vs.* RHE)	Tafel slope (mV dec^{-1})	Solution resistance, R_s (Ω)	Charge transfer resistance, R_{ct} (kΩ)
Bare GCE	> 400.0	–	12.81	5.14
Graphene	> 350.0	–	10.21	4.72
CoS_2/G	> 350.0	96.4	12.10	1.38
CoO_x/G	260.3	–	11.90	1.46
MoS_2/G	196.8	44.3	11.72	1.23
Co-MoS_2/G-5	78.1	40.0	8.01	0.36
10 wt.% Pt/C	46.9	32.2	7.78	0.12

and the resultant Co-MoS_2/G-5 exhibits improved HER efficiency than the undoped MoS_2/G catalyst. To provide the insights into the HER mechanism, Tafel plots were derived from LSV curves by fitting the linear segments to Tafel equation [69]:

$$\eta = b \log i + a \tag{1}$$

Here, η represents the overpotential, b is the Tafel slope, i is the current density, and a is a constant. According to Fig. 4c, a Tafel slope of 40.0 mV dec^{-1} is observed for Co-MoS_2/G-5 catalyst within an overpotential range of 50 – 200 mV, which is also very close to the value of 10 wt.% Pt/C catalyst (32.2 mV dec^{-1}). It also reveals that the Volmer–Heyrovsky mechanism takes place during the hydrogen evolution on the surface of Co-MoS_2/G-5 catalyst [70]. For a particular electrocatalytic system, it is always preferred to achieve lower Tafel slope, which indicates faster reaction taking place. Therefore, the lower Tafel slope of Co-MoS_2/G-5 than the CoS_2/G and MoS_2/G samples further confirms the enhanced catalytic activity after Co incorporation into MoS_2/G. This improved HER activity may also be attributed to the strong chemical and electronic coupling between Co-doped MoS_2 nanosheets and graphene network, resulting in fast electron kinetics between the catalyst and electrode surface.

This hypothesis was further confirmed by EIS measurements at an overpotential of 150 mV. As shown in Fig. 4d, in the high-frequency zone, both MoS_2/G and Co-MoS_2/G-5 exhibit one capacitive semicircle, inferring that the reaction is kinetically controlled. The electrical equivalent circuit diagram (shown in top right corner) is used to model the electrode/electrolyte interface, where the C_{dL} is associated to electrical double-layer capacitance, and W is corresponding to Warburg impedance. Though the solution resistance (R_s) values are almost similar for all catalyst samples, the Co-MoS_2/G-5 shows lower charge transfer resistance (R_{ct}) of 0.36 kΩ than other samples, except only 10 wt.% Pt/C (0.12 kΩ). Hence, much faster electron transfer is one of the key factors contributing to the superior HER kinetics for Co-MoS_2/G-5 catalyst. All major HER parameters are displayed in Table 2, measured from LSV and EIS analyses.

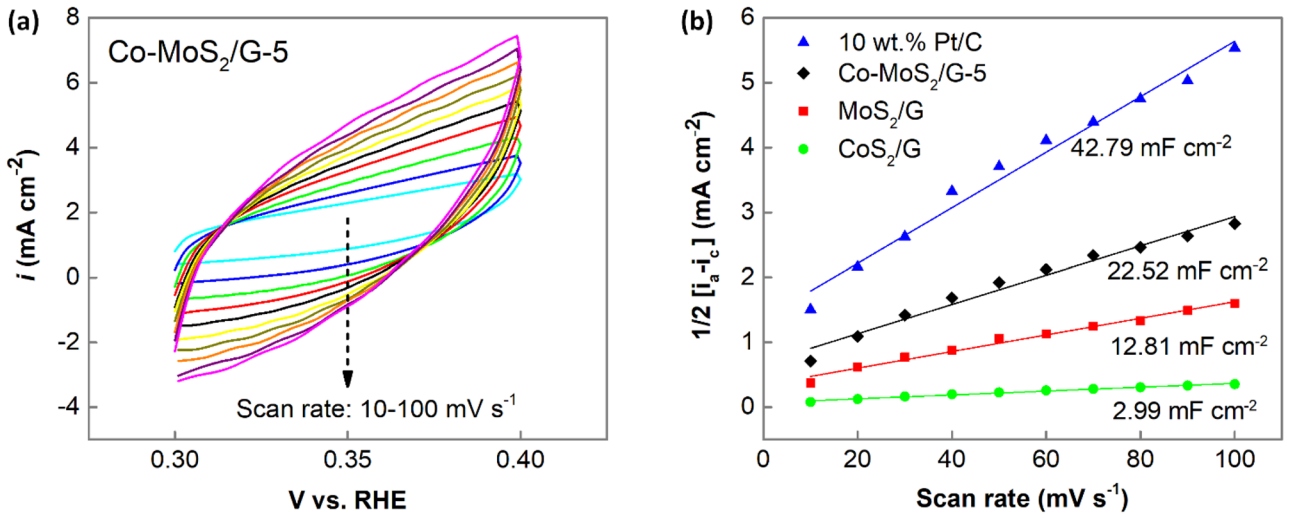

Fig. 5 CV curves of **a** Co-MoS_2/G-5 in a potential window without faradaic reaction at the scan rates of 10 – 100 mVs^{-1} in 0.5 M H_2SO_4. [CV curves for 10 wt.% Pt/C, MoS_2/G, and CoS_2/G samples are provided in Fig. S3 (supplementary information)]. **b** Subsequent EDLC measurements

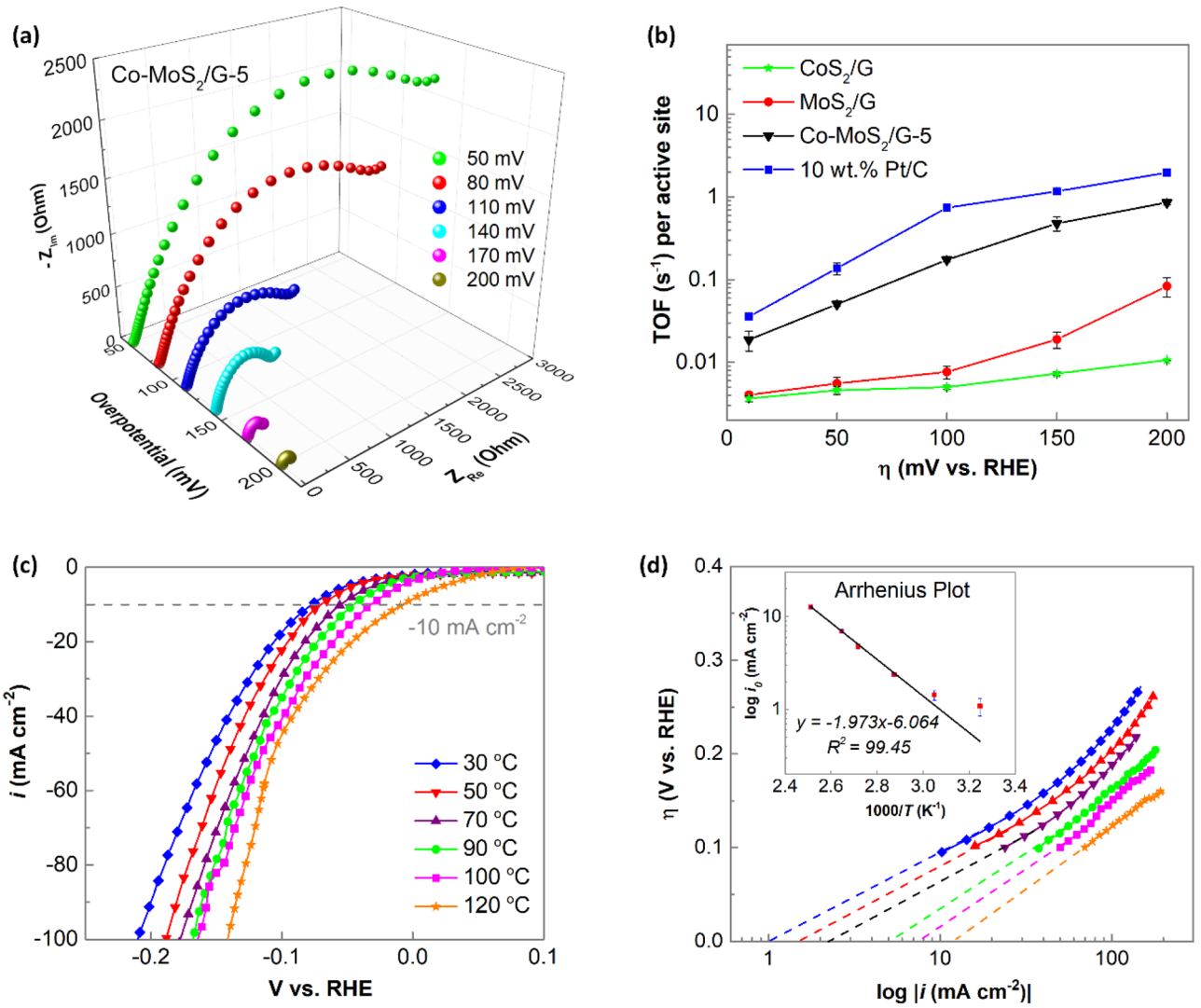

Fig. 6 **a** Nyquist plots showing the EIS responses of Co-MoS_2/G-5 at various overpotentials (50 – 200 mV). **b** TOF measurements of catalyst samples in the overpotential range of 10 – 200 mV. **c** LSVs of Co-MoS_2/G-5 within a temperature range of 30 – 120 ℃. **d** Corresponding Tafel slops [Inset: Arrhenius plot]

Moreover, the double-layer capacitance (C_{dl}) was measured to predict the electrochemically active surface area, by a simple cyclic voltammetry (CV) approach [41]. The CV measurements were performed within a potential range of 0.3 – 0.4 V *vs.* RHE as shown in Fig. 5a and Fig. S4a–c, where the currents are mainly ascribed to the charging of double layer at electrode/electrolyte interface. The measured C_{dl} values were recorded as a function of average capacitive current, $\frac{1}{2}(i_a - i_c)$ at 0.35 V *vs.* RHE within the scan rate of 10 – 100 mV s^{-1} in 0.5 M H_2SO_4 electrolyte. As displayed in Fig. 5b, the C_{dl} values of 10 wt.% Pt/C, Co-MoS_2/G-5, MoS_2/G, and CoS_2/G were calculated as 42.79, 22.52, 12.81, and 2.99 mF cm^{-2}, respectively, which reveals that the C_{dl} of Co-MoS_2/G-5 catalyst is approximately 2 times higher than the undoped MoS_2/G. These results clearly indicate the formation of defects due to Co-doping, which creates higher percentage of the active sites, further enhancing the HER activities.

In addition, Fig. 6a represents the Nyquist plots of Co-MoS_2/G-5 catalyst at various overpotentials of 50 – 200 mV. In this system, R_{ct} decreases significantly with increasing the overpotentials, from 3.96 kΩ at 50 mV to only 0.006 kΩ at 200 mV (Table S1, supporting information). Lower R_{ct} demonstrates faster electrocatalytic activity at higher overpotential. Besides, the exchange current density (i_0) is considered as another important parameter which is generally proportional to the active surface area of catalyst materials. The i_0 can be obtained from the linearized *Butler-Volmer equation* [43, 71]:

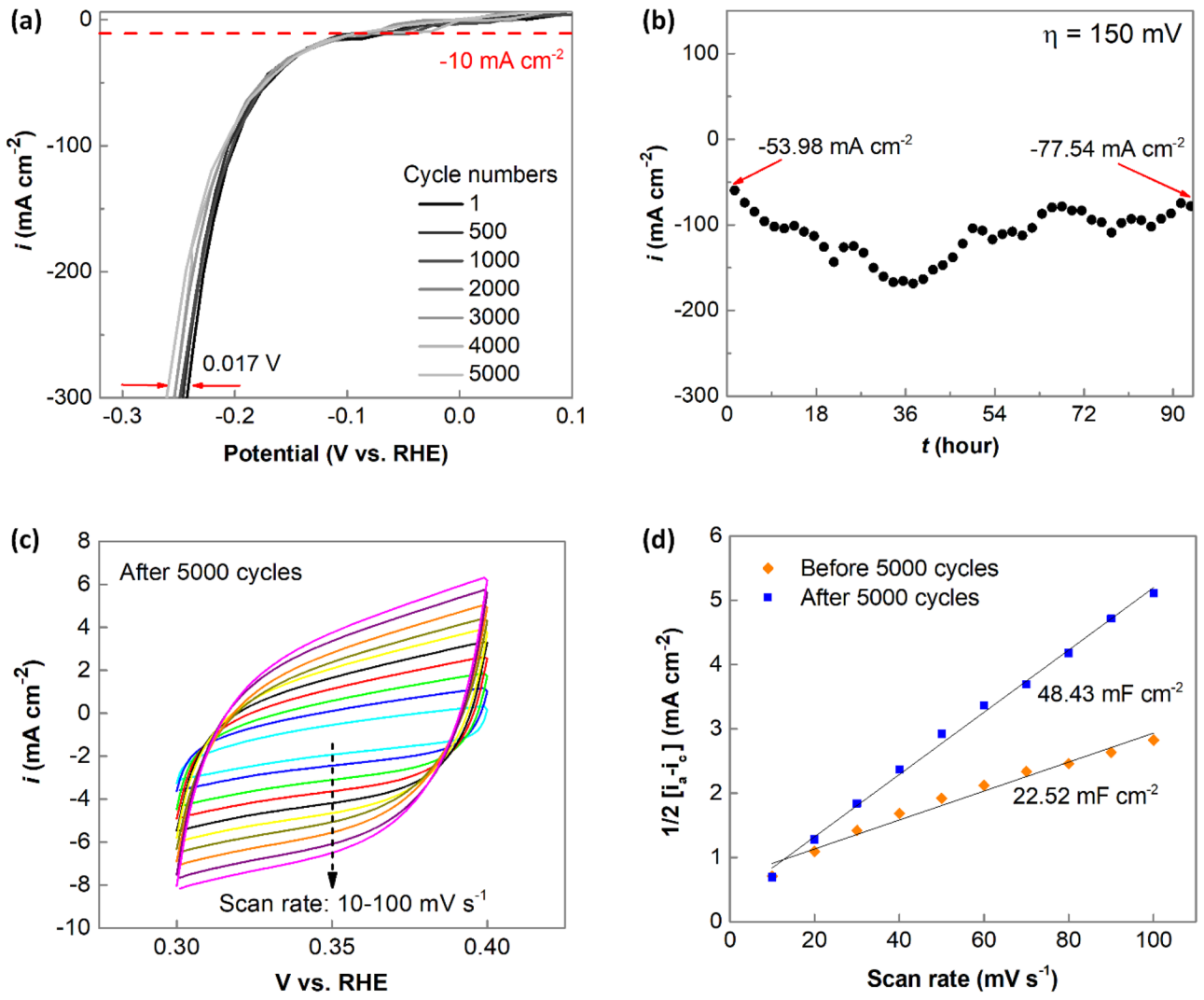

Fig. 7 **a** Polarization curves of Co-MoS_2/G-5 at a scan rate of 50 mV s^{-1} from 1 to 5000 cycles. **b** Constant potential electrolysis test for 94 h at 150 mV *vs.* RHE. **c** CVs of Co-MoS_2/G-5 catalyst after stability test in a potential window without faradaic reaction. **d** C_{dl} measurements of Co-MoS_2/G-5 before and after 5000 cycles

$$i_0 = \frac{RT}{nFAR_{ct}} \tag{2}$$

At low overpotential, the charge transfer reaction is assumed as a one-electron process ($n=1$), and the surface area (A) is assumed to be the geometric area (0.0707 cm^2) of catalyst coating. Considering the overpotential at 50 mV, the i_0 of Co-MoS_2/G-5 is thus found to be $i_0 = \frac{8.314\ \text{Jmol}^{-1}\text{K}^{-1}\times 298\ \text{K}}{1\times 96485.33\ \text{Cmol}^{-1}\times 0.0707\ \text{cm}^2\times 3960\Omega} = 0.0917\times 10^{-3}\text{Acm}^{-2}$.

In comparison, the Nyquist plots of 10 wt.% Pt/C catalyst are shown in Fig. S5 (supporting information), and based on the R_{ct} values from Table S1, the i_0 is calculated as 0.2115×10^{-3} A cm^{-2} at a low overpotential of 50 mV. Moreover, the turnover frequency (TOF) was determined for HER catalysts, which estimates the number of hydrogen molecules formed per active site of catalyst material per 1 s. If the cathodic current is considered solely designated to hydrogen evolution, TOF can be measured from the following relationship [72, 73]:

$$TOF = \frac{\text{No. of total hydrogen turn overs/cm}^2\ \text{geometric area}}{\text{No. of active sites/cm}^2\text{geometric area}} \tag{3}$$

Dai et al. described a simple electrochemical approach to measure the TOF values [41]. Based on their method, CV measurements (Fig. S6, supporting information) were performed for each of the catalyst samples in phosphate buffer (pH = 7) at a scan rate of 10 mV s^{-1}. Amount of charge (Q) was measured from the equation, $Q = \frac{CV\ Area}{Scan\ rate}$, and the number of active sites (n) was determined by $n = \frac{Q}{2F}$, where F is the Faraday constant. Finally, the $\text{TOF} = \frac{I}{nF}\times\frac{1}{2}$, where I represents the current (A) at

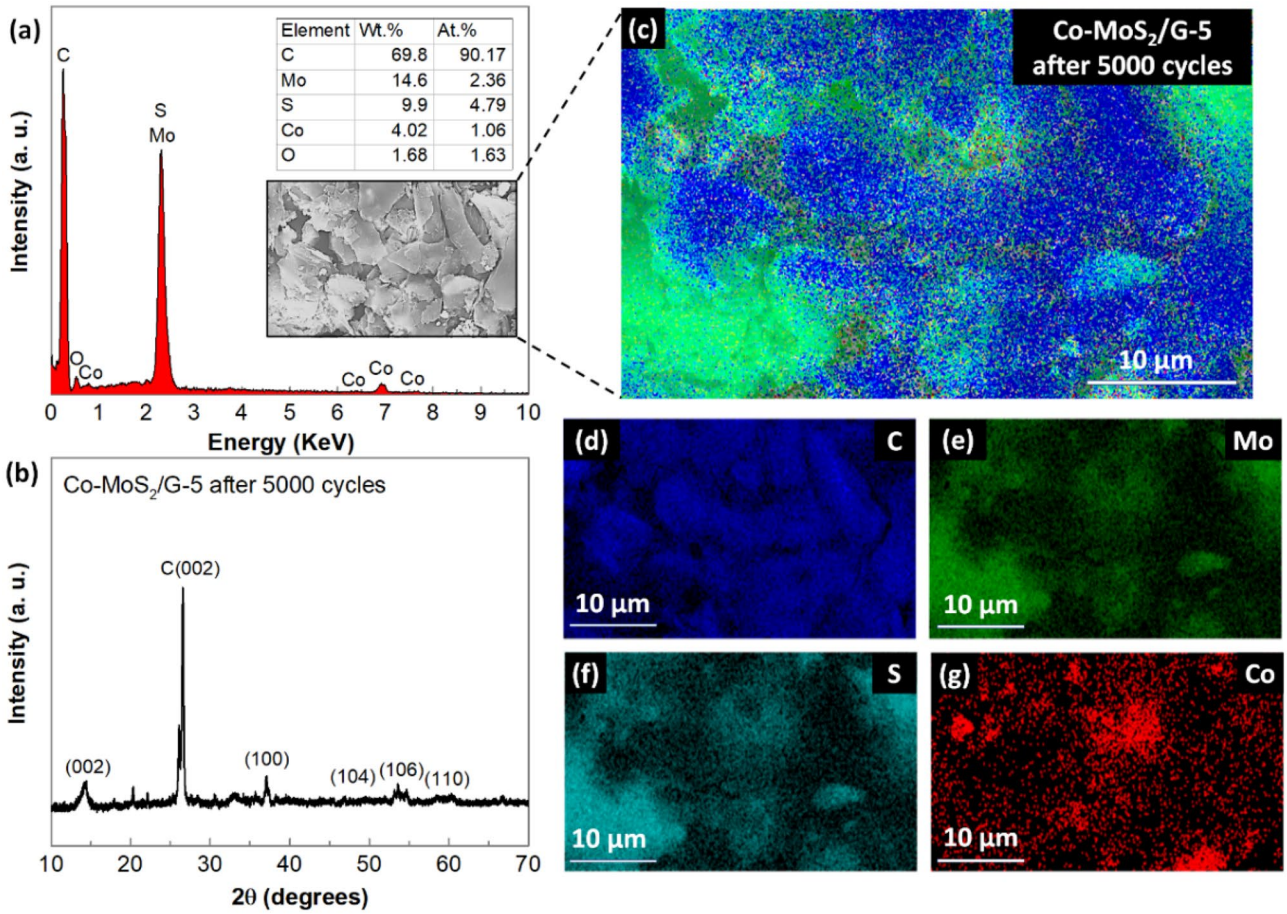

Fig. 8 Physical characterizations of Co-MoS_2/G-5 catalyst after stability test: **a** EDS elemental analysis. **b** XRD patterns. **c** EDS elemental mapping. **d**–**g** Elemental distributions of carbon (C), molybdenum (Mo), sulfur (S), and cobalt (Co) species, respectively

specific overpotential (η) during the LSV measurement in 0.5 M H_2SO_4. From Fig. 6b and Table S2, it can be clearly depicted that the TOF of Co-MoS_2/G-5 is higher than CoS_2/G and MoS_2/G catalysts within a wide range of overpotential (10 − 200 mV). Although the TOF of 10 wt.% Pt/C catalyst is much higher than the as-produced Co-MoS_2/G-5 nanocomposite, it is still very promising and comparable with previously reported values [41, 42].

Furthermore, the LSV tests were performed at a wide range of temperature from 30 to 120 ºC for Co-MoS_2/G-5 sample in 0.5 M H_2SO_4 electrolyte. Based on these results, the activation energy (E_a) can be measured by Arrhenius rate equation: $k = Ae^{-\frac{E_a}{RT}}$; [74] where k is the rate of reaction, A is the pre-exponential factor, R represents the universal gas constant, and T is the absolute temperature. In general, E_a is defined as the difference in electronic energy between the transition and initial states of catalyst materials, which is a key factor to determine the HER efficiency. As shown in Fig. 6c and d and Table S3 (supporting information), the HER activity improves with an increase in operating temperature by lowering the overpotentials and increasing exchange current density (i_0). The Arrhenius plot, $\log(i_0)$ *vs.* $\frac{1000}{T}$ was drawn (inset in Fig. 6d) based on the following equation:

$$\log\ i_0 = logA - \frac{E_a}{2.3\ RT} \tag{4}$$

where the rate of reaction (k) is signified by the exchange current density (i_0). The activation energy (E_a) was found to be 37.73 ± 1.26 kJ mol^{-1} or around 0.4 eV for Co-MoS_2/G-5 sample, which is very close to the value of platinum and other noble metal catalysts (20.0 to 40.0 kJ mol^{-1}) [75–77]. This low value of E_a also indicates that the higher HER activity of Co-MoS_2/G-5 catalyst was due to the higher intrinsic activity as well as the large surface area created from the defects of Co-doping.

The electrocatalytic stability is another key factor to assess a HER catalyst and to evaluate that, 5000 cycles of CV scanning were performed at a scan rate of 50 mV s^{-1} for Co-MoS_2/G-5 catalyst in the same acidic medium of 0.5 M H_2SO_4. Figure 7a displays the corresponding LSV curves, which indicates a small shift of overpotential (17 mV)

comparing to the initial curve at a high current density of −300 mA cm^{-2}. In addition, a continuous HER test was carried out at a constant potential of 150 mV *vs.* RHE, as shown in Fig. 7b. The high stability of Co-MoS_2/G-5 catalyst is demonstrated by the steady current for 94 h with a small shift from −53.98 to −77.54 mA cm^{-2}. The fluctuations in this time-dependent curve may originate from damage generations in the catalyst structure caused by the continuous formation of H_2 bubbles. In addition, double-layer capacitance (C_{dl}) was again measured after 5000 cycles of continuous HER test. Based on the results from Fig. 7c and d, it clearly demonstrates the increase in C_{dl} from 22.52 to 48.43 mF cm^{-2}, which confirms the activation of Co-MoS_2/G-5 taking place during the long run, due to the increase in surface area for excessive H_2 bubbling.

The Co-MoS_2/G-5 catalyst was further characterized after 5000 cycles of CV runs. As shown in Fig. 8a and b, the EDS and XRD results confirm the existence of Co-MoS_2 nanosheets intertwined with graphene, retaining the atomic ratio of Co: Mo: S as 0.45: 1.0: 2.0, which is almost similar to the initial values. Moreover, in Fig. 8c–g, the elemental distributions are displayed for C, Mo, S, and Co species, which confirms maintaining the uniform distribution of Co element in the Co-doped MoS_2 catalyst. Furthermore, the present findings were compared with the previously reported results of similar Co and/or Mo-based compounds, as shown in Table S4. In contrast with our new approach of ultrafast and facile microwave irradiation, most of the other compounds were manufactured by various complicated approaches. Additionally, it is noticeable that the present material exhibits low overpotential and a small Tafel slope, which are better than many other similar compounds.

4 Conclusions

In summary, the present study demonstrates an energy-efficient, ultrafast, and reliable microwave irradiation approach to synthesize the cobalt-doped molybdenum sulfide (Co-MoS_2) nanosheets uniformly distributed on graphene sheets. Among the resultant catalysts with different amounts of Co-loading, the Co-MoS_2/G-5 nanocomposite with an atomic ratio of Co: Mo: S is around 0.4: 1.0: 2.4 and delivers outstanding catalytic performance for hydrogen generation in acidic medium. The Co-MoS_2/G-5 catalyst reveals a low overpotential of 78.1 mV to reach 10 mA cm^{-2}, a small Tafel slope of 40.0 mV dec^{-1}, along with a high exchange current density of 0.0917 mA cm^{-2}. The resultant catalyst also demonstrates excellent stability both for 5000 cycles of CV test and 94 h constant potential test in acidic medium. These results clearly indicate that the formation of Co-Mo-S phase significantly increases the HER performance by promoting abundant defects, comparing to pure CoS_2 or pure MoS_2 phase. Moreover, the synergy of Co-MoS_2 with graphene network regulates both structural and electronic benefits, as well as the balance of active sites, and electronic conductivity. Following this simple microwave irradiation approach and the step-by-step characterization methods, other metal (Ni, Cu, Fe, Zn, etc.)-doped MoS_2 catalysts can be further studied, which possess immense potential in water electrolysis devices to stimulate the hydrogen gas production as a reliable future energy carrier.

Supplementary information The online version contains supplementary material available at https://doi.org/10.1007/s42114-022-00424-3.

Author contribution Conceptualization: Shatila Sarwar; methodology: Shatila Sarwar, Md Robayet Ahasan, Yifan Wang; formal analysis and investigation: Shatila Sarwar, Mao-Chia Lin; writing — original draft preparation: Shatila Sarwar; writing — review and editing: Xinyu Zhang, Ruigang Wang; funding acquisition: Xinyu Zhang; resources: Xinyu Zhang, Ruigang Wang; supervision: Xinyu Zhang, Ruigang Wang.

Funding This study was funded by the Auburn University-Intramural Grants Program (AU-IGP).

Declarations

Conflict of interest The authors declare no competing interests.

References

1. Dincer I, Zamfirescu C (2016) Hydrogen and its production. In: Sustainable Hydrogen Production. Elsevier, pp 65–97
2. Carmo M, Fritz DL, Mergel J, Stolten D (2013) A comprehensive review on PEM water electrolysis. Int J Hydrogen Energy 38:4901–4934. https://doi.org/10.1016/j.ijhydene.2013.01.151
3. Norskov JK, Christensen CH (2006) Toward efficient hydrogen production at surfaces. Science (80-) 312:1322–1323 . https://doi.org/10.1126/science.1127180
4. Anantharaj S, Noda S (2020) Amorphous catalysts and electrochemical water splitting: an untold story of harmony. Small 16:1–24. https://doi.org/10.1002/smll.201905779
5. Li X, Hao X, Abudula A, Guan G (2016) Nanostructured catalysts for electrochemical water splitting: current state and prospects. J Mater Chem A 4:11973–12000. https://doi.org/10.1039/c6ta02334g
6. Benck JD, Hellstern TR, Kibsgaard J, Chakthranont P, Jaramillo TF (2014) Catalyzing the hydrogen evolution reaction (HER) with molybdenum sulfide nanomaterials. ACS Catal 4:3957–3971. https://doi.org/10.1021/cs500923c
7. Zou X, Zhang Y (2015) Noble metal-free hydrogen evolution catalysts for water splitting. Chem Soc Rev 44:5148–5180. https://doi.org/10.1039/c4cs00448e
8. Gao X, Qi J, Wan S, Zhang W, Wang Q, Cao R (2018) Conductive molybdenum sulfide for efficient electrocatalytic hydrogen evolution. Small 14:1–9. https://doi.org/10.1002/smll.201803361
9. Sun H, Ma Z, Qiu Y, Liu H, Gao GG (2018) Ni@NiO nanowires on nickel foam prepared via "acid hungry" strategy: high supercapacitor performance and robust electrocatalysts for water splitting reaction. Small 14 https://doi.org/10.1002/smll.201800294

10. Nguyen QT, Nguyen PD, Nguyen D, Truong QD, Kim Chi TT, Ung TTD, Honma I, Liem NQ, Tran PD (2018) Novel amorphous molybdenum selenide as an efficient catalyst for hydrogen evolution reaction. ACS Appl Mater Interfaces 10:8659–8665. https://doi.org/10.1021/acsami.7b18675
11. Sarwar S, Ali A, Liu Z, Li J, Uprety S, Lee H, Wang R, Park M, Bozack MJ, Adamczyk AJ, Zhang X (2021) Towards thermoneutral hydrogen evolution reaction using noble metal free molybdenum ditelluride/graphene nanocomposites. J Colloid Interface Sci 581:847–859. https://doi.org/10.1016/j.jcis.2020.07.122
12. Handoko AD, Fredrickson KD, Anasori B, Convey KW, Johnson LR, Gogotsi Y, Vojvodic A, Seh ZW (2018) Tuning the basal plane functionalization of two-dimensional metal carbides (MXenes) to control hydrogen evolution activity. ACS Appl Energy Mater 1:173–180. https://doi.org/10.1021/acsaem.7b00054
13. Yuan S, Pang SY, Hao J (2020) 2D transition metal dichalcogenides, carbides, nitrides, and their applications in supercapacitors and electrocatalytic hydrogen evolution reaction. Appl Phys Rev 7 https://doi.org/10.1063/5.0005141
14. Noh SH, Hwang J, Kang J, Seo MH, Choi D, Han B (2018) Tuning the catalytic activity of heterogeneous two-dimensional transition metal dichalcogenides for hydrogen evolution. J Mater Chem A 6:20005–20014. https://doi.org/10.1039/c8ta07141a
15. Lin L, Sherrell P, Liu Y, Lei W, Zhang S, Zhang H, Wallace GG, Chen J (2020) Engineered 2D transition metal dichalcogenides—a vision of viable hydrogen evolution reaction catalysis. Adv Energy Mater 10 https://doi.org/10.1002/aenm.201903870
16. Chhowalla M, Shin HS, Eda G, Li LJ, Loh KP, Zhang H (2013) The chemistry of two-dimensional layered transition metal dichalcogenide nanosheets. Nat Chem 5:263–275. https://doi.org/10.1038/nchem.1589
17. Jaramillo TF, Jørgensen KP, Bonde J, Nielsen JH, Horch S, Chorkendorff I (2007) Identification of active edge sites for electrochemical H2 evolution from MoS2 nanocatalysts. Science (80-) 317:100–102 . https://doi.org/10.1126/science.1141483
18. Xie S, Sun B, Sun H, Zhan K, Zhao B, Yan Y, Xia BY (2019) Engineering of molybdenum sulfide nanostructures towards efficient electrocatalytic hydrogen evolution. Int J Hydrogen Energy 44:15009–15016. https://doi.org/10.1016/j.ijhydene.2019.04.106
19. Li Y, Wang H, Xie L, Liang Y, Hong G, Dai H (2011) MoS2 nanoparticles grown on graphene: an advanced catalyst for the hydrogen evolution reaction. J Am Chem Soc 133:7296–7299
20. Zhang N, Gan S, Wu T, Ma W, Han D, Niu L (2015) Growth Control of MoS2 nanosheets on carbon cloth for maximum active edges exposed: an excellent hydrogen evolution 3d cathode. ACS Appl Mater Interfaces 7:12193–12202. https://doi.org/10.1021/acsami.5b02586
21. Huang H, Chen L, Liu C, Liu X, Fang S, Liu W, Liu Y (2016) Hierarchically nanostructured MoS2 with rich in-plane edges as a high-performance electrocatalyst for the hydrogen evolution reaction. J Mater Chem A 4:14577–14585. https://doi.org/10.1039/c6ta06174e
22. Kibsgaard J, Chen Z, Reinecke BN, Jaramillo TF (2012) Engineering the surface structure of MoS2 to preferentially expose active edge sites for electrocatalysis. Nat Mater 11:963–969. https://doi.org/10.1038/nmat3439
23. Liu L, Li X, Xu LC, Liu R, Yang Z (2017) Effect of edge structure on the activity for hydrogen evolution reaction in MoS 2 nanoribbons. Appl Surf Sci 396:138–143. https://doi.org/10.1016/j.apsusc.2016.10.137
24. Tahira A, Ibupoto ZH, Mazzaro R, You S, Morandi V, Natile MM, Vagin M, Vomiero A (2019) Advanced electrocatalysts for hydrogen evolution reaction based on core-shell MoS2/TiO2 nanostructures in acidic and alkaline media. ACS Appl Energy Mater 2:2053–2062. https://doi.org/10.1021/acsaem.8b02119
25. Han X, Tong X, Liu X, Chen A, Wen X, Yang N, Guo XY (2018) Hydrogen evolution reaction on hybrid catalysts of vertical MoS2 nanosheets and hydrogenated graphene. ACS Catal 8:1828–1836. https://doi.org/10.1021/acscatal.7b03316
26. Nguyen VT, Le PA, Hsu YC, Wei KH (2020) Plasma-induced exfoliation provides onion-like graphene-surrounded MoS2 nanosheets for a highly efficient hydrogen evolution reaction. ACS Appl Mater Interfaces 12:11533–11542. https://doi.org/10.1021/acsami.9b20902
27. Behranginia A, Asadi M, Liu C, Yasaei P, Kumar B, Phillips P, Foroozan T, Waranius JC, Kim K, Abiade J, Klie RF, Curtiss LA, Salehi-Khojin A (2016) Highly efficient hydrogen evolution reaction using crystalline layered three-dimensional molybdenum disulfides grown on graphene film. Chem Mater 28:549–555. https://doi.org/10.1021/acs.chemmater.5b03997
28. Zhang S, Yang H, Gao H, Cao R, Huang J, Xu X (2017) One-pot synthesis of CdS irregular nanospheres hybridized with oxygen-incorporated defect-rich MoS2 ultrathin nanosheets for efficient photocatalytic hydrogen evolution. ACS Appl Mater Interfaces 9:23635–23646. https://doi.org/10.1021/acsami.7b03673
29. Liu Y, Zeng C, Ai L, Jiang J (2019) Boosting charge transfer and hydrogen evolution performance of CdS nanocrystals hybridized with MoS 2 nanosheets under visible light irradiation. Appl Surf Sci 484:692–700. https://doi.org/10.1016/j.apsusc.2019.03.327
30. Yu SH, Tang Z, Shao Y, Dai H, Wang HY, Yan J, Pan H, Chua DHC (2019) In situ hybridizing MoS2 microflowers on VS2 microflakes in a one-pot CVD process for electrolytic hydrogen evolution reaction. ACS Appl Energy Mater 2:5799–5808. https://doi.org/10.1021/acsaem.9b00928
31. Deng J, Li H, Xiao J, Tu Y, Deng D, Yang H, Tian H, Li J, Ren P, Bao X (2015) Triggering the electrocatalytic hydrogen evolution activity of the inert two-dimensional MoS2 surface via single-atom metal doping. Energy Environ Sci 8:1594–1601. https://doi.org/10.1039/c5ee00751h
32. Li R, Yang L, Xiong T, Wu Y, Cao L, Yuan D, Zhou W (2017) Nitrogen doped MoS2 nanosheets synthesized via a low-temperature process as electrocatalysts with enhanced activity for hydrogen evolution reaction. J Power Sources 356:133–139. https://doi.org/10.1016/j.jpowsour.2017.04.060
33. Lin C, Gao Z, Jin J (2019) Boosting alkaline hydrogen evolution activity with Ni-doped MoS 2/reduced graphene oxide hybrid aerogel. Chemsuschem 12:457–466. https://doi.org/10.1002/cssc.201802488
34. Lukowski MA, Daniel AS, Meng F, Forticaux A, Li L, Jin S (2013) Enhanced hydrogen evolution catalysis from chemically exfoliated metallic MoS2 nanosheets. J Am Chem Soc 135:10274–10277. https://doi.org/10.1021/ja404523s
35. Liu Q, Fang Q, Chu W, Wan Y, Li X, Xu W, Habib M, Tao S, Zhou Y, Liu D, Xiang T, Khalil A, Wu X, Chhowalla M, Ajayan PM, Song L (2017) Electron-doped 1T-MoS2 via interface engineering for enhanced electrocatalytic hydrogen evolution. Chem Mater 29:4738–4744. https://doi.org/10.1021/acs.chemmater.7b00446
36. Merki D, Vrubel H, Rovelli L, Fierro S, Hu X (2012) Fe Co, and Ni ions promote the catalytic activity of amorphous molybdenum sulfide films for hydrogen evolution. Chem Sci 3:2515–2525. https://doi.org/10.1039/c2sc20539d
37. Bonde J, Moses PG, Jaramillo TF, Norskov JK, Chorkendorff I (2008) Hydrogen evolution on nano-particulate transition metal sulfides. Faraday Discuss 140:219–231. https://doi.org/10.1039/b814058h
38. Rheem Y, Park SH, Han Y, Lee K-H, Choi S-M, Myung NV (2019) Electrospun cobalt-doped MoS 2 nanofibers for electrocatalytic hydrogen evolution. J Electrochem Soc 166:F996–F999. https://doi.org/10.1149/2.1041912jes

39. Wu L, Xu X, Zhao Y, Zhang K, Sun Y, Wang T, Wang Y, Zhong W, Du Y (2017) Mn doped MoS 2 /reduced graphene oxide hybrid for enhanced hydrogen evolution. Appl Surf Sci 425:470–477. https://doi.org/10.1016/j.apsusc.2017.06.223
40. Dong T, Zhang X, Wang P, Chen HS, Yang P (2020) Formation of Ni-doped MoS2 nanosheets on N-doped carbon nanotubes towards superior hydrogen evolution. Electrochim Acta 338:135885. https://doi.org/10.1016/j.electacta.2020.135885
41. Dai X, Du K, Li Z, Liu M, Ma Y, Sun H, Zhang X, Yang Y (2015) Co-doped MoS2 nanosheets with the dominant CoMoS phase coated on carbon as an excellent electrocatalyst for hydrogen evolution. ACS Appl Mater Interfaces 7:27242–27253. https://doi.org/10.1021/acsami.5b08420
42. Bose R, Seo M, Jung CY, Yi SC (2018) Comparative investigation of the molybdenum sulphide doped with cobalt and selenium towards hydrogen evolution reaction. Electrochim Acta 271:211–219. https://doi.org/10.1016/j.electacta.2018.03.151
43. Ma J, Cai A, Guan X, Li K, Peng W, Fan X, Zhang G, Zhang F, Li Y (2020) Preparation of ultrathin molybdenum disulfide dispersed on graphene via cobalt doping: a bifunctional catalyst for hydrogen and oxygen evolution reaction. Int J Hydrogen Energy 45:9583–9591. https://doi.org/10.1016/j.ijhydene.2020.01.176
44. Bhorde A, Waykar R, Rondiya SR, Nair S, Lonkar G, Funde A, Dzade NY, Jadkar S (2021) Structural, electronic, and optical properties of lead-free halide double perovskite Rb2AgBiI6: a combined experimental and density functional theory study. ES Mater Manuf 12:43–52 https://doi.org/10.30919/esmm5f1042
45. Ahmed R, Wang S, Rehman S, Sun J, Wang J, Si R, Zhu A, Yu Y, Li Q (2021) Maxwell-Wagner relaxation in Ca- , Sm- and Nd-doped Ceria. 95–104
46. Wang D, Guo Z (2020) Ten years' glory of halide perovskite materials. Engineered 11:1–2. https://doi.org/10.1002/pip.2404
47. Liang H, Zhang X, Lin B, Wang F, Cheng Z, Shi X, Guene Lougou B (2020) Design of biomimetic leaf-type hierarchical nanostructure for enhancing the solar energy harvesting of ultra-thin perovskite solar cells. ES Energy Envirofile///C/Users/Shatila/OneDrive - Auburn Univ Co-doped HER Catal Compos Hybrid Mater 10:22–33 https://doi.org/10.30919/esee8c728
48. Li Q (2021) Compositional engineering of halide perovskites. ES Mater Manuf 12:1–2. https://doi.org/10.1021/ja809598r
49. Khan SH, Pathak B, Fulekar MH (2020) A study on the influence of metal (Fe, Bi, and Ag) doping on structural, optical, and antimicrobial activity of ZnO nanostructures. Adv Compos Hybrid Mater 3:551–569. https://doi.org/10.1007/s42114-020-00174-0
50. Yin X, Yan Y, Miao M, Zhan K, Li P, Yang J, Zhao B, Xia BY (2018) Quasi-emulsion confined synthesis of edge-rich ultrathin MoS2 nanosheets/graphene hybrid for enhanced hydrogen evolution. Chem - A Eur J 24:556–560. https://doi.org/10.1002/chem.201703493
51. Huang J, Chen M, Li X, Zhang X, Lin L, Liu W, Liu Y (2019) A facile layer-by-layer fabrication of three dimensional MoS 2 -rGO-CNTs with high performance for hydrogen evolution reaction. Electrochim Acta 300:235–241. https://doi.org/10.1016/j.electacta.2019.01.107
52. Guo Y, Gan L, Shang C, Wang E, Wang J (2017) A cake-style CoS2@MoS2/RGO hybrid catalyst for efficient hydrogen evolution. Adv Funct Mater 27:1–7. https://doi.org/10.1002/adfm.201602699
53. Zhao J, Wei D, Zhang C, Shao Q, Murugadoss V, Guo Z, Jiang Q, Yang X (2021) An overview of oxygen reduction electrocatalysts for rechargeable zinc-air batteries enabled by carbon and carbon composites. Eng Sci 15:1–19 https://doi.org/10.30919/es8d420
54. Vijeata A, Chaudhary GR, Umar A, Chaudhary S (2021) Distinctive solvatochromic response of fluorescent carbon dots derived from different components of aegle marmelos plant. Eng Sci 15:197–209 https://doi.org/10.30919/es8e512
55. Mirabootalebi SO (2020) A new method for preparing buckypaper by pressing a mixture of multi-walled carbon nanotubes and amorphous carbon. Adv Compos Hybrid Mater 3:336–343. https://doi.org/10.1007/s42114-020-00167-z
56. Wu N, Du W, Hu Q, Vupputuri S, Jiang Q (2021) Recent development in fabrication of co nanostructures and their carbon nanocomposites for electromagnetic wave absorption. Eng Sci 13:11–23 https://doi.org/10.30919/es8d1149
57. Yu Z, Bai Y, Wang JH, Li Y (2021) Effects of functional additives on structure and properties of polycarbonate-based composites filled with hybrid chopped carbon fiber/graphene nanoplatelet fillers. ES Energy Environ 12:66–76 https://doi.org/10.30919/esee8c434
58. Islam MJ, Rahman MJ, Mieno T (2020) Safely functionalized carbon nanotube–coated jute fibers for advanced technology. Adv Compos Hybrid Mater 3:285–293. https://doi.org/10.1007/s42114-020-00160-6
59. Hong H, Gao L, Zheng Y, Xing X, Sun F, Liu T, Murugadoss V, Guo Z, Yang M, Zhang H (2021) A path of multi-energy hybrids of concentrating solar energy and carbon fuels for low CO2 emission. ES Energy Environ 13:1–7 https://doi.org/10.30919/esee8c520
60. Sun J, Zhang X, Du Q, Murugadoss V, Wu D, Guo Z (2021) The contribution of conductive network conversion in thermal conductivity enhancement of polymer composite: a theoretical and experimental study. ES Mater Manuf 13:53–65 https://doi.org/10.30919/esmm5f450
61. Sarwar S, Nautiyal A, Cook J, Yuan Y, Li J, Uprety S, Shahbazian-Yassar R, Wang R, Park M, Bozack MJ, Zhang X (2020) Facile microwave approach towards high performance MoS2/graphene nanocomposite for hydrogen evolution reaction. Sci China Mater 63:62–74. https://doi.org/10.1007/s40843-019-9555-0
62. Sarwar S, Ali A, Wang Y, Ahasan MR, Wang R, Adamczyk AJ, Zhang X (2021) Enhancement of hydrogen evolution reaction activity using metal−rich molybdenum sulfotelluride with graphene support: a combined experimental and computational stuDY. Nano Energy 90:106599. https://doi.org/10.1016/j.nanoen.2021.106599
63. Zheng F, Huang N, Peng R, Ding Y, Li G, Xia Z, Sun P, Sun X, Geng J (2018) Cobalt-doped molybdenum disulfide in-situ grown on graphite paper with excellent electrocatalytic activity for triiodide evolution. Electrochim Acta 263:328–337. https://doi.org/10.1016/j.electacta.2018.01.054
64. Lendzion-Bielun Z, Narkiewicz U, Arabczyk W (2013) Cobalt-based catalysts for ammonia decomposition Materials (Basel) 6:2400–2409. https://doi.org/10.3390/ma6062400
65. Ahn S, Yang J, Lim H, Shin HS (2016) Selective synthesis of pure cobalt disulfide on reduced graphene oxide sheets and its high electrocatalytic activity for hydrogen evolution reaction. Nano Converg 3:2–8. https://doi.org/10.1186/s40580-016-0066-x
66. Huang N, Peng R, Ding Y, Yan S, Li G, Sun P, Sun X, Liu X, Yu H (2019) Facile chemical-vapour-deposition synthesis of vertically aligned co-doped MoS2 nanosheets as an efficient catalyst for triiodide reduction and hydrogen evolution reaction. J Catal 373:250–259. https://doi.org/10.1016/j.jcat.2019.04.007
67. Fan J, Ekspong J, Ashok A, Koroidov S, Gracia-Espino E (2020) Solid-state synthesis of few-layer cobalt-doped MoS2 with CoMoS phase on nitrogen-doped graphene driven by microwave irradiation for hydrogen electrocatalysis. RSC Adv 10:34323–34332. https://doi.org/10.1039/d0ra05560c
68. Wu Q, Zhu Y, Guo J, Wang S, Feng X, Chen Z (2021) Insight into the influence of doped oxygen on active sites of molybdenum sulfide materials in hydrogen evolution reaction. Int J Hydrogen Energy 1–10 https://doi.org/10.1016/j.ijhydene.2021.01.019
69. Morales-Guio CG, Stern LA, Hu X (2014) Nanostructured hydrotreating catalysts for electrochemical hydrogen evolution. Chem Soc Rev 43:6555–6569. https://doi.org/10.1039/c3cs60468c

70. Zhou W, Jia J, Lu J, Yang L, Hou D, Li G, Chen S (2016) Recent developments of carbon-based electrocatalysts for hydrogen evolution reaction. Nano Energy 28:29–43. https://doi.org/10.1016/j.nanoen.2016.08.027
71. Newman J, Thomas-Alyea KE (2004) Electrochemical systems
72. Merki D, Fierro S, Vrubel H, Hu X (2011) Amorphous molybdenum sulfide films as catalysts for electrochemical hydrogen production in water. Chem Sci 2:1262–1267. https://doi.org/10.1039/c1sc00117e
73. Kibsgaard J, Jaramillo TF (2014) Molybdenum phosphosulfide: an active, acid-stable, earth- Abundant catalyst for the hydrogen evolution reaction. Angew Chemie - Int Ed 53:14433–14437. https://doi.org/10.1002/anie.201408222
74. Kim H, Kim J, Han GH, Guo W, Hong S, Park J, Ahn SH (2021) Electrodeposited rhenium–cobalt alloy with high activity for acidic hydrogen evolution reaction. J Ind Eng Chem 95:357–366. https://doi.org/10.1016/j.jiec.2021.01.008
75. Huff C, Biehler E, Quach Q, Long JM, Abdel-Fattah TM (2021) Synthesis of highly dispersive platinum nanoparticles and their application in a hydrogen generation reaction. Colloids Surfaces A Physicochem Eng Asp 610:125734. https://doi.org/10.1016/j.colsurfa.2020.125734
76. Yuan M, Cui Z, Yang J, Cui X, Tian M, Xu D, Ma J, Dong Z (2017) Ultrafine platinum nanoparticles modified on cotton derived carbon fibers as a highly efficient catalyst for hydrogen evolution from ammonia borane. Int J Hydrogen Energy 42:29244–29253. https://doi.org/10.1016/j.ijhydene.2017.09.178
77. Durst J, Simon C, Hasché F, Gasteiger HA (2015) Hydrogen oxidation and evolution reaction kinetics on carbon supported Pt, Ir, Rh, and Pd electrocatalysts in acidic media. J Electrochem Soc 162:F190–F203. https://doi.org/10.1149/2.0981501jes